Korean J. Chem. Eng., 33(3), 1014-1027 (2016)
DOI: 10.1007/s11814-015-0206-8

pISSN: 0256-1115
eISSN: 1975-7220

Prediction of power consumption and performance in ultrafiltration of simulated latex effluent using non-uniform pore sized membranes

Amira Abdelrasoul†, Huu Doan, Ali Lohi, and Chil-Hung Cheng

Department of Chemical Engineering, Ryerson University, 350 Victoria Street, Toronto, Ontario M5B 2K3, Canada
(*Received 7 May 2015 • accepted 30 September 2015*)

Abstract−Tha aim of the present study was to develop a series of numerical models for an accurate prediction of the power consumption in ultrafiltration of simulated latex effluent. The developed power consumption model incorporated fouling attachment, as well as chemical and physical factors in membrane fouling, in order to ensure accurate prediction and scale-up. This model was applied to heterogeneous membranes with non-uniform pore sizes at a given operating conditions and mem- brane surface charges. Polysulfone flat membrane, with a membrane molecular weight cutoff (MWCO) of 60,000 dalton, at different surface charges was used under a constant flow rate and cross-flow mode. In addition, the developed models were examined using various membranes at a variety of surface charges so as to test the overall reliability and accuracy of these models. The power consumption predicted by the models corresponded to the calculated values from the experimental data for various hydrophilic and hydrophobic membranes with an error margin of 6.0% up to 19.1%.

Keywords: Modeling, Power Consumption, Membrane Fouling, Transmembrane Pressure, Ultrafiltration

INTRODUCTION

Low-pressure membranes have been used for a variety of industrial applications due to their abilities in producing drinking water, as well as facilitating the treatment of wastewater that meets or even exceeds stringent industry standards. Despite relative research and market success, membrane fouling is a serious constraint currently preventing more widespread application of ultrafiltration in cases with diversified range of contaminants. Membrane fouling likewise increases operational costs due to permeate flux decline and increased power consumption caused by the higher transmembrane pressure (TMP) [1-3]. In addition, frequent chemical cleaning of membranes with fouling leads to a rapid deterioration of the membrane's overall performance, a shortened service time, and an increased production and use cost. Notably, for application cases with a longer period of filtration, membrane fouling is not completely reversible by back-washing [4]. As a result, efficient power consumption ultrafiltration process is becoming a necessity for feasible long- and short-term monetary returns.

According to the 2002 American Water Works Association Research Foundation (AWWARF) survey, the capital cost for a low pressure membrane system is in the range of $ 0.18-$ 0.23/ gallon per day (gpd), a number expected to decline to $ 0.15-$ 0.20/gpd in the coming decades [5]. Further reduction in cost would largely stem from the development of higher flux, lower fouling membranes, or more efficient ways of operating membrane systems. Various research projects on this subject indicate that the implementation of different fouling remediation techniques can result in a significant reduction of the filtration process power consumption [6-8]. For a plant capable of producing 100 m^3/day of water, the energy consumption is more than 10 KWh/m^3; however, this number can be reduced to 3.5 KWh/m^3 if the fouling is adequately controlled [9]. One research study shows that the total energy consumed for 40 minutes of water filtration ranged from 50.08 to 62.54 kJ/L at 3 bar, while the energy consumed in membrane cleaning ranged from 87.08 to 107 kJ for the duration of 50-100 minutes at different operational pressures [10].

What is of interest here is that power consumption models have the potential to predict the power consumption trends, as well as provide accurate predictions of the power consumption for larger-scale ultrafiltration systems. While there is a variety of relevant power consumption data available for analyzing and modeling purposes [11-13], there are no adequate predictive models for an accurate estimation of the power consumption in ultrafiltration of latex effluent using different types of heterogeneous membranes, featuring a diverse range of materials and a variety of MWCO values at the required levels of performance. This absence of sophisticated predictive models could be attributed to the fact that the increase in transmembrane pressure through the filtration is dependent on the mass of fouling. As a consequence, the average transmembrane pressure through the filtration process will vary with the fouling attachments and the morphological membrane characterization [14-16]. Thus, analysis and modeling of the experimental data reported in research literature is generally system specific and insufficient for an accurate prediction when implemented under alternative conditions. The extent to which existing studies can be used is likewise limited in terms of process generalization and scale-up. It was determined that operation conditions, latex solution chemistry, and surface charge also have a significant impact on fouling attachments, the total mass of fouling, and the cake height, a set

†To whom correspondence should be addressed.
E-mail: amira.abdelrasoul@ryerson.ca

correlations that have been showcased in our previous publications [14-18]. Thus, the average transmembrane pressure of the filtration processes varies on a case by case basis. In fact, the prediction of power consumption is more accurate when based on the variation of the transmembrane pressure throughout the filtration process. In our previous studies a mathematical model was developed to predict the mass of fouling using a homogeneous and heterogeneous membranes with uniform and non-uniform pore sizes for the ultrafiltration of latex paint solution, and featuring a wide range of particle size distribution values [19,20]. This mathematical model accounts for the existing chemical attachments in membrane fouling and incorporates the coupled effects of chemical and physical factors involved in membrane fouling, and allows for a comprehensive understanding of the fouling phenomenon. This mathematical model was able to accurately predict the increase in transmembrane pressure and the mass of the fouling retained by the membranes. Additional predictive models were likewise developed and validated for the accurate estimation of fouling attachments at a given operating condition and membrane surface charge, as can be referred to in our previous publication [15]. The goal of the current study was to enable accurate prediction of the specific power consumption in the ultrafiltration process of simulated latex effluent using heterogeneous membranes at a given feed flow rate, initial transmembrane pressure, feed concentration, and membrane surface charge for a required cumulative permeate volume per unit area. The increase in the transmembrane pressure will be predicted based on the morphological characterization of the membrane as well as its fouling attachments. The examined experimental models were validated using different types of heterogeneous membranes, and then validated using experimental data from treated membrane surface charges with different zeta potential values. The influence of the operating conditions on specific power consumption for heterogeneous membranes was also investigated in detail.

ATTACHMENT MATHEMATICAL MODEL

A mechanistic model was successfully developed for the deposition of non-uniform latex particles in heterogeneous and non-uniform pore size membranes [20]. The fouling was considered as related to the attachments between foulant and the membrane surface (depositional attachment), and the attachments among foulant entities (coagulation attachment). This mechanistic model was based on the fouling potential mechanisms of various particle sizes and their capacity to get attached to membranes with non-uniform pore sizes. In the developed attachment model, the sizes of the latex particles and membrane pores were considered as the primary factors in determining the occurrence of surface fouling (cake layer formation or pore blocking) and adsorptive internal plugging (pore constriction). A heterogeneous membrane had the pore size distribution of (N) non-uniform pore sizes. The possible attachments of each particle size range were accordingly applied in the mathematical model for every available pore size of (i). Eventually, the average percentage (x_i) of each pore size (i), estimated by ImageJ software, was used in the model. To examine the validity and reliability of the model, monodisperse particles with sizes of 50 nm and 100 nm and the simulated latex effluent were used. According to these mathematical expressions, the mass of the particles contributing to pore blocking can be calculated by using Eq. (1), while the mass of the particles accountable for the cake layer can be estimated by Eq. (2). These equations are functions of the membrane's physical properties, feed concentration, particle's projected area, attachment fouling probabilities, and cumulative filtration volume per unit area. The sum of m_p and m_c stands for the total mass of fouling retained by the membrane (m_t).

$$\begin{aligned} m_p = {} & \Sigma_{i=1}^{N} x_i \left\{ \frac{\alpha_{pm}\varepsilon_s}{4^{\alpha_{pp}}\sigma_L}\left[1-\exp(-4^{\alpha_{pp}}\sigma_L C_f V_s)\right]\right\} \\ & + \Sigma_{i=1}^{N} x_i \left\{ \frac{N_m}{\sigma_{xs}\alpha_{pm}B_i}\left\{ \frac{\pi D_{m_i} L_m B_i \alpha_{pm}}{\tau} \right.\right. \\ & \left.\left. - \ln\left[1+\exp\left(\frac{\pi D_{m_i} L_m B_i \alpha_{pm}}{\tau} - \frac{\sigma_{xs}\alpha_{pm}B_i}{N_m} C_f V_s\right)\right]\right\}\right\} \\ & + \Sigma_{i=1}^{N} x_i \left\{ \frac{\alpha_{pm}\varepsilon_s}{\sigma_s}\left[1-\exp(-\sigma_s C_f V_s)\right]\right\} \end{aligned} \tag{1}$$

$$\begin{aligned} m_c = {} & \alpha_{pp} C_f V_s - \left\{ \Sigma_{i=1}^{N} x_i \left\{ \frac{\alpha_{pm}\varepsilon_s}{4^{\alpha_{pp}}\sigma_L}\left[1-\exp(-4^{\alpha_{pp}}\sigma_L C_f V_s)\right]\right\}\right\} \\ & + \Sigma_{i=1}^{N} x_i \left\{ \frac{N_m}{\sigma_{xs}\alpha_{pm}B_i}\left\{ \frac{\pi D_{m_i} L_m B_i \alpha_{pm}}{\tau} - \ln\left[1+\exp\left(\frac{\pi D_{m_i} L_m B_i \alpha_{pm}}{\tau} \right.\right.\right.\right. \\ & \left.\left.\left.\left. - \frac{\sigma_{xs}\alpha_{pm}B_i}{N_m} C_f V_s\right)\right]\right\}\right\} + \Sigma_{i=1}^{N} x_i \left\{ \frac{\alpha_{pm}\varepsilon_s}{\sigma_s}\left[1-\exp(-\sigma_s C_f V_s)\right]\right\} \\ = {} & \alpha_{pp} C_f V_s + \left\{ \frac{\alpha_{pm}(1-\varepsilon_s)-\alpha_{pp}}{4^{\alpha_{pp}}}\left[\frac{\left[1-\exp(-4^{\alpha_{pp}}\sigma_L C_f V_s)\right]}{\sigma_L} \right.\right. \\ & \left.\left. + \frac{\left[1-\exp(-4^{\alpha_{pp}}\sigma_s C_f V_s)\right]}{\sigma_s}\right]\right\} \end{aligned} \tag{2}$$

where m_p [kg/m^2] is the total mass of particles attached to membrane pores per unit membrane surface area, m_c [kg/m^2] is the total mass of particles in the cake layer per unit membrane surface area, x_i is the average percentage of the pore of size i, N is the number of the non-uniform pore sizes determined in the pore size distribution of the heterogeneous membranes, α_{pp} [dimensionless] is the coagulation attachment probability which represents the particle-to-particle attachment, α_{pm} [dimensionless] is the depositional attachment which represents the particle-to-membrane attachment, ε_s [dimensionless] is the membrane surface porosity, D_{m_i} [m] is the membrane pore diameter of size i, B_i [m^{-2}] is the mass transfer coefficient, σ_L [m^2/kg] is the projected area of a unit mass of the large particles on the membrane surface, σ_s [m^2/kg] is the projected area of a unit mass of the small particles on the membrane surface, σ_{xs} [m^2/kg] is the projected area of a unit mass of the very small particles on the membrane surface. Moreover, a [m] is the particle radius, of which details about its classification can be found in Section 2 of our previous study [20]. N_m is the number density of membrane pores per unit membrane surface area, L_m [m] is the length of a membrane pore, τ is tortuosity of the membrane porous structure [20], C_f [kg/m^3] is the mass concentration of particles in the feed, and V_s [m^3/m^2] is the cumulative volume of the permeate normalized to membrane surface area. The mean

average of particle size was used for the projected area calculations for each size range. The tortuosity in our study was estimated by using the Hagen Poiseuille equation and the experimental data of the permeate flux of water collected at different transmembrane pressures as expressed in our previous study [20]. Eqs. (1) and (2) are solved for α_{pp} and α_{pm} using m_p and m_c values that have been measured experimentally, as described in our previous study [20]. In addition, the increase in the transmembrane membrane pressure during a filtration process normalized to that of clean membrane can be calculated from Eq. (3) below:

$$P' = 1 + \frac{1}{1-\sigma_L \Sigma_{i=1}^{N} x_i m_{pL_i}} + \frac{1}{1-\sigma_S \Sigma_{i=1}^{N} x_i m_{pS_i}} + \frac{1}{\left(1-\frac{\Sigma_{i=1}^{N} x_i m_{w_i}}{\rho L_m}\right)^2} + \frac{\hat{R}_c}{R_m}[\alpha_{pp} C_f V_s - (\Sigma_{i=1}^{N} x_i m_{pL_i} - \Sigma_{i=1}^{N} x_i m_{pS_i} - \Sigma_{i=1}^{N} x_i m_{w_i})] \quad (3)$$

where m_{pL_i} [kg/m^2] is the mass of the particles larger than the pore of size i contributing to the pore blocking, as represented in Eq. (4), m_{pS_i} [kg/m^2] is the mass of the small particles contributing to the blocking of the pores of size i, as represented in Eq. (5), and m_{w_i} [kg/m^2] is the mass of particles attached to the pore wall of size i, as represented in Eq. (6). Lastly, R_m [m^{-1}] is the membrane's resistance, while $\hat{R}_c$ [m/kg] is the resistance due to the cake layer.

$$m_{pL_i} = \frac{\alpha_{pm}\varepsilon_s}{4^{\alpha_{pp}}\sigma_L}[1-\exp(-4^{\alpha_{pp}}\sigma_L C_f V_s)] \quad (4)$$

$$m_{pS_i} = \frac{\alpha_{pm}\varepsilon_s}{\sigma_s}[1-\exp(-\sigma_s C_f V_s)] \quad (5)$$

$$m_{w_i} = \frac{N_m}{\sigma_{xs}\alpha_{pm}B_i}\left\{\frac{\pi D_{m_i} L_m B_i \alpha_{pm}}{\tau} - \ln\left[1+\exp\left(\frac{\pi D_{m_i} L_m B_i \alpha_{pm}}{\tau} - \frac{\sigma_{xs}\alpha_{pm}B_i}{N_m} C_f V_s\right)\right]\right\} \quad (6)$$

In our recent publication, numerical models were further developed to predict the depositional and coagulation attachments at a given operating condition, as well as the membrane surface charges [15]. The fouling attachment models agreed well with the experimental values in the transmembrane pressure range of 5.00 to 45.00 psia, feed flow rate range of 1.50 to 7.50 LPM, feed concentration range of 0.26 to 2.34 kg/m^3, and zeta potential of membrane surface in range of −50.00 to −10.00 mV. These models were validated by using various heterogeneous membranes featuring different materials, MWCO values, and surface charges. The predicted attachment probabilities can in turn be used to estimate the mass of fouling using the summation of Eq. (1) and Eq. (2), and the increase in transmembrane pressure from Eq. (3) from the developed fouling model.

$$\alpha_{pm} = +0.22 + 0.0528 * \text{TMP [psia]} - 0.0112 * \text{Q [LPM]} + 0.0804 * C_f \text{[kg/m}^3\text{]} + 0.025 * \zeta \text{[mV]} \quad (7)$$

$$\alpha_{pp} = +0.30 + 0.025 * \text{TMP [psia]} - 0.069 * \text{Q [LPM]} + 0.082 * C_f \text{[kg/m}^3\text{]} + 1\times10^{-7} * \zeta \text{[mV]} \quad (8)$$

where TMP [psia] is the transmembrane pressure, Q [LPM] is the feed flow rate, and ζ [mV] is the zeta potential of the membrane surface.

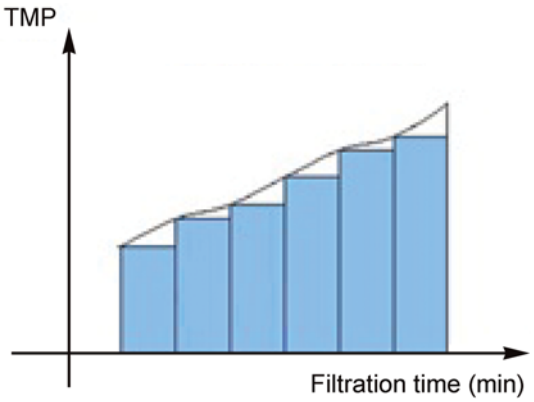

Fig. 1. Area under the curve represents $\overline{TMP}_{AVG}$ [psia·min].

SPECIFIC POWER CONSUMPTION

The resistance to permeate flow during the filtration process would increase due to the pore blockage and cake layer formation, eventually resulting in membrane fouling. As a consequence, the permeate flux declines with filtration time. A higher level of permeate flux can be attained by increasing the transmembrane pressure, causing a higher energy consumption. In this case, the specific power consumption per unit volume of filtrate is defined as follows:

$$\text{Specific power consumption}\left[\frac{\text{kWh}}{\text{m}^3}\right] = 1.916\times10^{-6}\times\frac{\overline{TMP}_{AVG} * Q}{\overline{V}_s} \quad (9)$$

where $\overline{TMP}_{AVG}$ is the time-averaged transmembrane pressure throughout the filtration duration. $\overline{TMP}_{AVG}$ [psia·min] can be calculated based on the area under the curve, as shown in Fig. 1. Q [LPM] is the feed flow rate, and $\overline{V}_s$ [m^3] is the cumulative permeate volume.

MATERIALS AND METHOD

1. Experimental Set-up and Procedure

Fig. 2 shows a schematic diagram of the experimental setup. A comprehensive account of the experiment setup, experimental procedure, membrane filtration unit, and latex paint used can be found in our previous study [19]. The current study mostly used polysulfone membranes with MWCO of 60,000 (GE Water & Process Technologies). Ultrafilic membranes with MWCO of 100,000 (GE Water & Process Technologies), cellulose acetate membranes with MWCO of 20,000 (GE Water & Process Technologies), and polyvinylidene difluoride (PVDF) membranes with MWCO of 100,000 (Koch Membrane Systems) were likewise tested to evaluate the level of predictability and accuracy of the correlations developed for the generalized application with different heterogeneous membranes featuring distinct surface charges. Table 1 shows the membrane

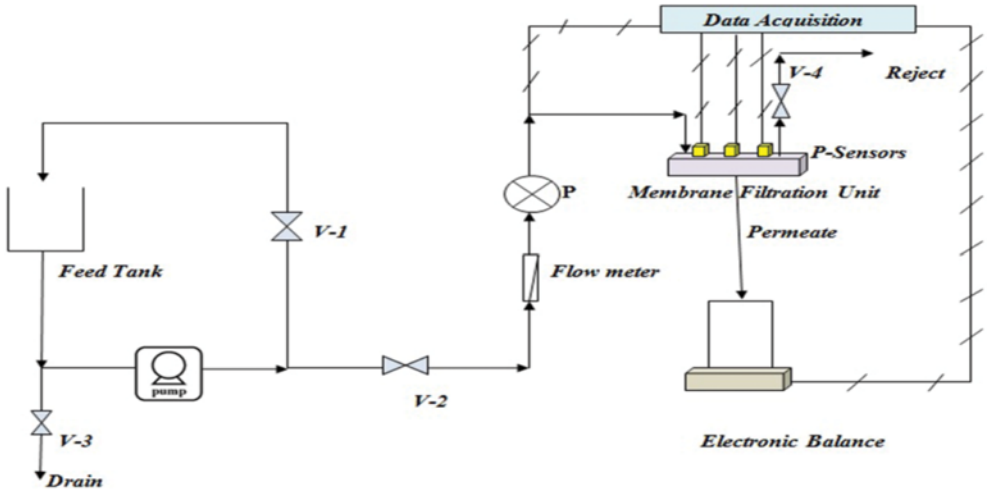

Fig. 2. Schematic diagram of experimental set-up.

Table 1. Performance characteristics of nonuniform membranes

Membrane	MWCO	Pore density[a] [pore/cm^2]	Typical flow rate[b] [mL/min/cm^2]	τ	R_m [m^{-1}]	Zeta potential of the membrane surface [mV]
PS	60,000	7×10^8	2.5	1.5	1.34E+11	−42.40
CA	20,000	5×10^7	0.2	1.3	1.71E+12	−33.90
Ultrafilic	100,000	6×10^8	2.9	1.6	1.89E+10	−41.50
PVDF	100,000	4×10^8	1.1	1.65	1.15E+11	−2.50

[a]Tolerance ±15%

[b]Initial flow rates measured using pre-filtered water at 10 Psi

characteristics. The zeta potential values of the untreated membranes implemented in the study were −42.40 mV, −41.50 mV, −2.50 mV, and −33.90 mV for polysulfone, ultrafilic, PVDF, and cellulose acetate membranes, respectively. Furthermore, the models obtained in this study were examined using the membranes at different surface charge values to test the accuracy and the reliability of the models for practical cases where the surface charge of the membrane could differ from its value for the clean and untreated membrane. The membrane surface charge was adjusted using a solution in an MPT-2 autotitrator of the zeta potential analyzer (Zetasizer-Nano Series, Malvern Instruments Ltd, UK, ±0.01 MV). Further details on the procedure developed for changing the membrane surface charge and testing its stability were described extensively in our recent publication [15]. For these experiments, a simulated latex effluent with a fixed pH value of 7 was used in all experimental runs. The zeta potential of latex particles at a pH of 7 was approximately −26.61 mV.

The total mass of fouling (m_t) is the difference in weight of the membrane before and after filtration. For measuring the mass of particles contributing to cake layer (m_c), the cake was scratched off under a microscope, so as to keep the membranes pores blocked with the particles contributing to the pore blocking. The scratched off solid portion was then weighted to determine the amount of cake layer. The blocked pores of the membrane were checked using SEM. The mass of particles contributing to pore blocking (m_p), is the difference between the weight of the membrane before filtration (clean membrane) and the weight after the cake layer was scratched off. The mass of particles (m_t, m_c and m_p) was measured using an electronic balance (Mettler Toledo Model AB 54-S Fact, Switzerland, ±0.1 mg). Fig. 3(a) presents SEM images of the membrane surface after the ultrafiltration of the latex solution, and before the cake layer was scratched off, which represents the total mass of solids (m_t). The SEM image of the membrane surface after the cake layer was scratched off for the measurments of m_c and m_p, as shown in Fig. 3(b). As clarified by a higher magnification in Fig. 3(c), the particles blocked the membrane pores and were trapped inside the membrane matrix.

2. Analytical Methods

A zeta potential analyzer (ZetasizerNano Series, Malvern Instruments Ltd, UK, ±0.01 mV) was used to measure the zeta potential values [mV] of the latex particles and membrane surface. As described in Section 4.1 [20], the ImageJ software [ImageJ 1.46r, National Institutes of Health, USA] was used for the estimation of the pore size distributions in heterogeneous membranes. A more comprehensive account of the instruments and procedures used for handling solid content, scanning electron microscope (SEM), and particle size distribution of latex paint dispersions of different concentrations was included in previous work [19].

3. Experimental Design and Statistical Method

For this study, the central composite face-centered CCF response surface method (RSM) was used in the experimental design [21]. The specific power consumption is the main focus. The process

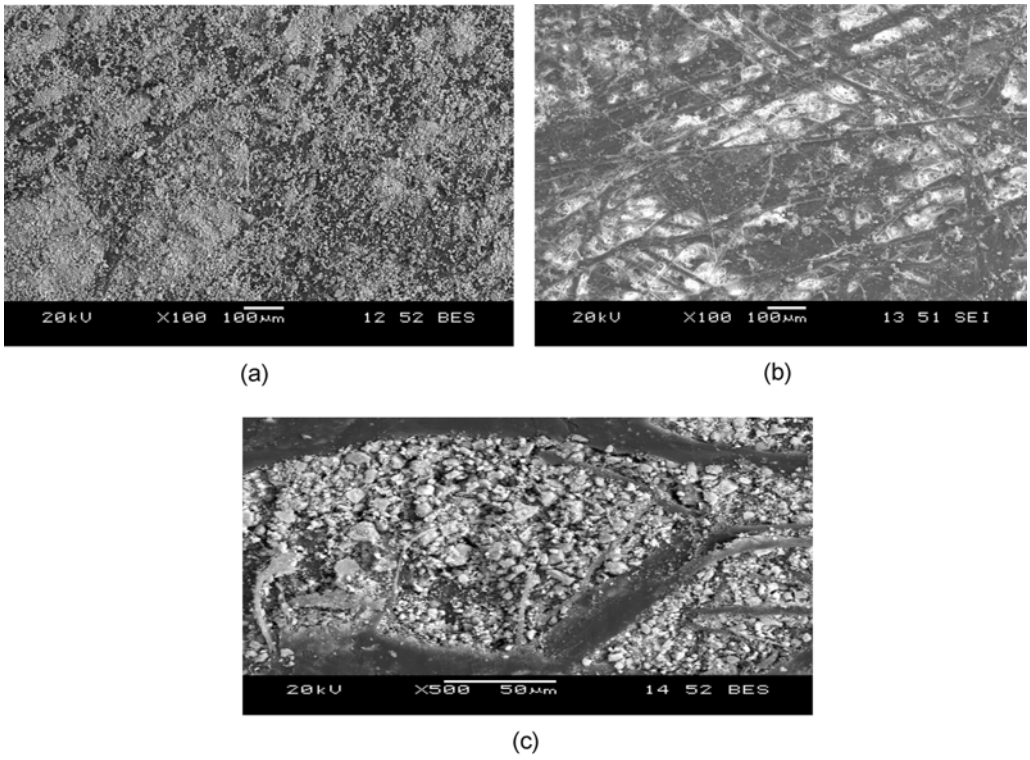

Fig. 3. The SEM images of membrane surface after ultrafiltration: (a) Before the cake layer was scratched off; (b) after the cake layer was scratched off for the mass of fouling contributed to (m_p); (c) after scratching off the cake layer at a higher magnification of 500.

Table 2. Process parameter levels

Factor	Variable	Range		Unit
		Low	High	
		(−1)	(+1)	
TMP	Initial transmembrane pressure	15.00	35.00	psia
Q	Feed flow rate	1.00	7.00	LPM
C_f	Feed concentration	0.78	1.82	kg/m^3

parameters include transmembrane pressure, feed flow rate, and feed concentration, as indicated in Table 2. The operating parameter levels were selected based on the concentration of the actual latex effluent, the transmembrane pressure and the feed flow rate used in the industrial application and could be applicable with lab scale setting. Table 3 outlines the total mass of fouling and the specific power consumption at the coded and actual levels of the process parameters. The coded values are assigned as −1 (low), 0 (medium), and 1 (high). Twenty experiments were conducted, and their results were then analyzed using multi-regression. To minimize error, six experiments at zero code for each process parameter were replicated in randomized order. The solution temperature was maintained at room temperature (22-24 °C). The ultrafiltration time for each experiment was kept consistent (25 minutes) so that the impact of the operating conditions on the total mass of fouling, fouling attachments, and cumulative filtration volume per unit area could be examined. As a result, the effect of fouling on specific power consumption was accurately investigated. Statistical software (Stat-Ease, Version 8.0 Stat-Ease Inc., USA) was used to determine the best-fitting model by regression and stepwise elimination. The coefficients for a full model were assessed through regression analysis and then tested for their importance. To assess the significance of the coefficients, the F-test was implemented, after which the insignificant coefficients were accordingly excluded. P-value analysis was used to set the level of confidence for the F-test, while the analysis of variance (ANOVA) and coefficients of determination (R^2) were employed to evaluate the model fitting.

The linear model can be expressed as Eq. (10) below:

$$Y = \beta_{ko} + \Sigma_{i=1}^{N} \beta_{ki} x_i \quad (10)$$

where Y is the response factor of the specific power consumption, x_i the ith independent factor, β_{ko} the intercept, β_{ki} the first-order model coefficients.

RESULTS AND DISCUSSION

1. The Effects of Operating Conditions on Power Consumption

During this section of the experiment, each operating condition and its respective influences were conducted at the average range value for the other process parameters presented in Table 2. At a feed flow rate of 4.00 L/min and a feed concentration of 1.30 kg/m^3, an increase of transmembrane pressure from 15.00 to 45.00 psia led to an increase in the total mass of fouling from 0.011 kg/m^2 to 0.018 kg/m^2, as shown in Fig. 4. When the transmembrane pressure was raised from 15.00 to 45.00 psia, the volumetric permeate flux, respectively, increased from 0.0089 m^3/m^2 to 0.0139

Table 3. Experimental parameters and results based on the experimental design for the mass of fouling and the specific power consumption

Exp. No.	TMP			Independent Variables		m_t [kg/m^2]	Power consumed [kW·h/m^3]
	Initial TMP [psia]	TMP_{AVG}* [psia]	Final TMP [psia]	Feed flow rate Q [LPM]	Feed concentration C_f [kg/m^3]		
1	15.00 (−1)	15.50	16.00	1.00 (−1)	0.78 (−1)	0.0031	1.65
2	35.00 (1)	35.60	36.50	1.00 (−1)	0.78 (−1)	0.0052	2.64
3	15.00 (−1)	15.20	15.50	7.00 (1)	0.78 (−1)	0.0025	1.92
4	35.00 (1)	36.20	37.00	7.00 (1)	0.78 (−1)	0.008	3.58
5	15.00 (−1)	15.60	16.00	1.00 (−1)	1.82 (1)	0.0044	3.44
6	35.00 (1)	36.00	37.00	1.00 (−1)	1.82 (1)	0.008	4.28
7	15.00 (−1)	16.50	18.00	7.00 (1)	1.82 (1)	0.0093	4.55
8	35.00 (1)	38.20	41.00	7.00 (1)	1.82 (1)	0.015	7.67
9	15.00 (−1)	16.70	18.00	4.00 (0)	1.30 (0)	0.0114	1.59
10	35.00 (1)	38.20	41.00	4.00 (0)	1.30 (0)	0.0178	3.25
11	25.00 (0)	28.60	32.00	1.00 (−1)	1.30 (0)	0.0195	0.85
12	25.00 (0)	26.10	27.00	7.00 (1)	1.30 (0)	0.0088	3.33
13	25.00 (0)	26.00	27.00	4.00 (0)	0.78 (−1)	0.011	1.50
14	25.00 (0)	26.80	31.00	4.00 (0)	1.82 (1)	0.0167	8.00
15	25.00 (0)	25.50	30.00	4.00 (0)	1.30 (0)	0.0135	2.04
16	25.00 (0)	27.90	30.00	4.00 (0)	1.30 (0)	0.0135	2.03
17	25.00 (0)	27.80	30.00	4.00 (0)	1.30 (0)	0.0135	1.98
18	25.00 (0)	27.90	30.00	4.00 (0)	1.30 (0)	0.0135	1.99
19	25.00 (0)	27.90	30.00	4.00 (0)	1.30 (0)	0.0135	2.04
20	25.00 (0)	27.80	30.00	4.00 (0)	1.30 (0)	0.0135	1.98

*TMP_{AVG} [psia]=$\overline{TMP}_{AVG}$ [psia·min]/Filtration time [min], $\overline{TMP}_{AVG}$ [psia·min] calcualted as mentioned in section 3

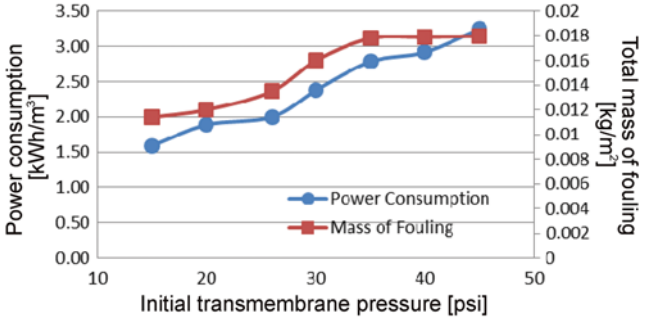

Fig. 4. Effect of initial transmembrane pressure at [Q=4.00 LPM] and [C_f=1.30 kg/m^3] on the total mass of fouling and specific power consumption using untreated polysulfone membranes with surface charge of −42.40 mV.

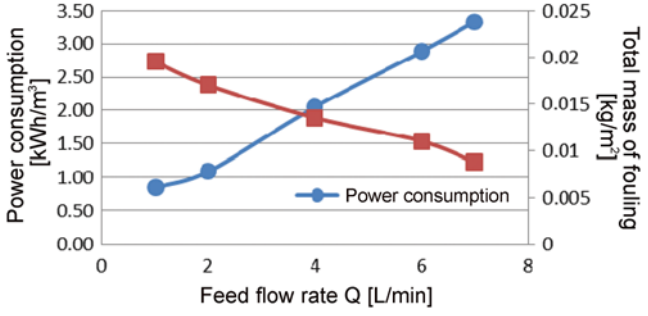

Fig. 5. Effect of feed flow rate at [TMP=25.00 psia], and [C_f=1.30 kg/m^3] on total mass of fouling and power consumption using untreated polysulfone membranes with surface charge of −42.40 mV.

m^3/m^2. The higher permeate flow occurring through the membrane brought additional particles to the membrane's surface, and as a consequence the chances for particle-to-particle and particle-to-membrane collision and attachment increased, causing higher attachment probabilities. The coagulation (α_{pp}) and the depositional (α_{pm}) attachments increased from 0.54 to 0.82 and 0.67 to 0.91, respectively. This increase in the total mass of fouling, in turn, facilitated an increase in the transmembrane pressure through the ultrafiltration process from 3.00 to 6.00 psia, and raised the specific power consumption from 1.59 to 3.25 kW·h/m^3, as illustrated in Fig. 4.

Fig. 5 depicts the effect of the feed flow rate on the total mass of fouling and the specific power consumption at 25.00 psi and feed concentration of 1.30 kg/m^3. Increasing the feed flow rate from 1.00 LPM (cross flow velocity of 10.4 cm/s) to 7.00 LPM (cross flow velocity of 72.8 cm/s) caused a substantial decrease in the mass of fouling from 0.0195 to 0.0088 kg/m^2. At a higher flow rate, a higher shear rate is applied on the particles at the cake layer. A substantial decrease in fouling combined with the increase of the flow rate was expected to occur due to the shear-induced process of particles being washed away, as in the case of the homogeneous polycarbonate membrane discussed earlier [20]. Nevertheless, the overall results indicate that the increase in feed flow rate caused a

slight reduction in the coagulation attachment (α_{pp}) from 0.83 at 1.00 LPM to 0.70 at 7.00 LPM, in comparison to the results obtained with a polycarbonate uniform pore size membrane [17]. This particular experimental result may be attributed to the structure of the polysulfone membranes. Specifically, even at the highest flow rate of 7.00 LPM used in this research study, the particles were still actively attached to each other and contributing to the multiple cake layers inside the matrix of the membrane. On the other hand, at a higher flow rate, the cumulative permeate per unit area increased from 0.006 to 0.014 m^3/m^2. As a result, more particles came into contact with the membrane, leading to an increase in collisions and attachments between particles and the membrane's surface. In this case, the depositional attachment (α_{pm}) decreased only from 0.90 to 0.82 at 1.00 LPM and 7.00 LPM. The decrease in the total mass of fouling facilitated a smaller raise in the transmembrane pressure through the ultrafiltration duration from 7.00 to 2.00 psia. The power consumption per unit volume was raised from 0.85 to 3.33 kW·h/m^3 as illustrated in Fig. 5. This experimental trend agrees with Eq. (7) where the specific power consumption is directly proportional to the feed flow rate.

The effects of feed concentration on the total mass of fouling and the specific power consumption at a feed flow rate of 4.00 L/min and a transmembrane pressure of 25.00 psia can be seen in Fig. 6. Increasing the feed concentration resulted in a higher chance of particle-to-particle collision, which in turn enhanced the coagulation attachment probability and cake layer build up. As a consequence, the total mass of fouling increased from 0.011 kg/m^2 to 0.017 kg/m^2 when the concentration was raised from 0.78 kg/m^3 to 1.82 kg/m^3. The experiment showed that increasing the feed concentration from 0.78 kg/m^3 to 1.82 kg/m^3 led to a significant increase in the coagulation attachment probability, α_{pp}, from 0.34 to 0.81, and a slight increase in the depositional attachment probability, α_{pm}, from 0.83 to 0.89. Over the duration of the filtration process the transmembrane pressure was likewise raised from 3.00 to 7.00 psia when the feed concentration increased from 0.78 kg/m^3 to 1.82 kg/m^3 due to the increase in the total mass of fouling, as discussed in Section 3. The specific power consumption also increased from 1.50 kW·h/m^3 to 8.00 kW·h/m^3. Increasing the feed concentration resulted in a higher chance of particle-to-particle collision, a dynamic which enhanced the coagulation attachment probability and cake layer build. Alternatively, increasing the feed concentration from 0.78 kg/m^3 to 1.30 kg/m^3 led to a significant decrease in the volumetric permeate flux (V_s) from 0.0142 m^3/m^2 to 0.0114 m^3/m^2 due to the pore blockage. Further increase in the feed concentration from 1.30 kg/m^3 to 1.82 kg/m^3 produced a noticeable decrease in the volumetric permeate flux from 0.0114 m^3/m^2 to 0.00924 m^3/m^2. A reduced permeate flow through the membrane pores would decrease particle-to-membrane collision and attachment, allowing the depositional attachment probability, α_{pm}, to decrease as well. The reduced cumulative permeate volume could be attributed to the pore blockage and cake layer build-up that were increased due to the augmented feed concentration. Note that the specific power consumption is directly proportional to the increase in transmembrane pressure and inversely proportional to the cumulative permeate volume, as can be viewed in Eq. (9). In addition to the diminished cumulative permeate volume, the significant increase of the total mass of fouling due to feed concentration resulted in higher power consumption, caused by the higher transmembrane pressure. As shown in Fig. 6, a more noticeable increase in the power consumption occurred at the concentrations above 1.30 kg/m^3.

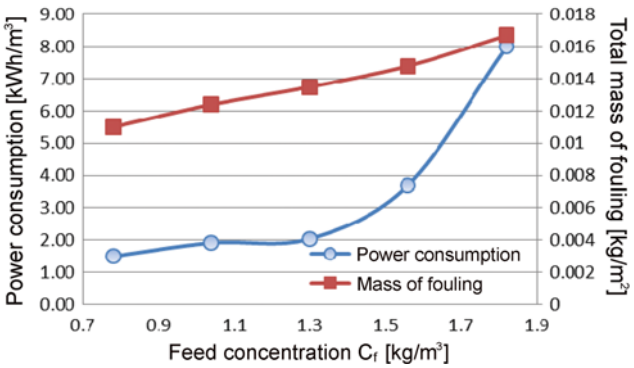

Fig. 6. Effect of feed concentration at [Q=4.00 LPM] and [TMP= 25.00 psia] on the total mass of fouling and the power consumption using untreated polysulfone membranes with surface charge of −42.40 mV.

2. Statistical Analysis

The central composite face-centered (CCF) response surface method (RSM) was selected in the current study as the optimal experimental design method. Within the framework of the study twenty experiments were performed, and the specific power consumption was accurately calculated for each of the experimental runs, as indicated in Table 3. The coded values are assigned as −1 (low), 0 (medium), and 1 (high), as indicated in Table 2. The results indicate that the specific power consumption varied between the ranges of 0.85 kW·h/m^3 to 8.00 kW·h/m^3.

Based on the ANOVA analysis and the multiregression method, the experimental data of specific power consumption was found to accurately correspond with the linear model. Eq. (9) presents a numerical model with the coefficient of determination (R^2) of 0.96. Notably, specific power consumption value occurring during the use of the polysulfone heterogeneous membranes was not significantly affected by the various interactions between the operating conditions.

$$\text{The specific power consumption} = -1.7280 + 0.1880 * TMP_{AVG} + 0.1872 * Q + 0.4900 * C_f \quad (11)$$

where the specific power consumption was function of average transmembrane pressure (TMP_{AVG}) [psia], feed flow rate (Q) [LPM], and feed concentration (C_f) [kg/m^3]. To assess their validity, the generated results were then analyzed by the ANOVA and presented in Table 4. The p-value indicates the probability value used to set the level of confidence for the F-test, as well as to ascertain the importance of each coefficient. According to the regression coefficients and probability values (p-value) shown in Table 4, the operating conditions (initial transmembrane pressure, feed flow rate, and feed concentration) noticeably affected the calculated power consumption.

The final transmembrane pressure can be predicted by using the initial transmembrane pressure value and the increase of trans-

Table 4. Regression coefficients and probability values of statistical analysis

Coded factor	Actual factor	Coefficient for specific power consumption [kW·h/m^3]	P-value
TMP_{AVG}	Average transmembrane pressure through the filtration process [psia]	0.1880	<0.0001
Q	Feed flow rate [LPM]	0.1872	0.0042
C_f	Feed concentration [kg/m^3]	0.4900	<0.0001

Values of "p-value" less than 0.05 indicate model terms are significant
In case of the specific power consumption model: TMP_{AVG}, Q, C_f are significant model terms

membrane pressure (P′) over the time estimated from Eq. (3). The predicted final transmembrane pressure can then be used to calculate the average transmembrane pressure TMP_{AVG} [psia], which in turn allows one to predict the specific power consumption from Eq. (11). The increase in the transmembrane pressure can be estimated from the morphological characterization of the membrane and the fouling attachments, as indicated in Eq. (3). Predictive models that offer an accurate estimation of the fouling attachments at a given operating condition and of the membrane surface charge values were recently developed and validated, as illustrated in Eq. (7) and Eq. (8) respectively.

The influence of the transmembrane pressure, feed flow rate, and feed concentration on the fouling attachment can be seen in Table 3. For instance, experimental runs (1&2), (3&4), (5&6), (7&8) and (9&10) reflect the effects of the transmembrane pressure, experimental runs (1& 3), (2&4), (5&7), (6&8) and (11&12) indicate the influences of the feed flow rate, while experimental runs (1&5), (2&6), (3&7), (4&8) and (13&14) showcase the effects of feed concentration. Increasing the transmembrane pressure, feed flow rate, or raising the feed concentrations, caused an increase in the specific power consumption. Regression coefficients in Eq. (11) reflect the extent to which each operating condition can have an impact on the power consumption, as described in Table 4. Of particular interest to our experimental direction here is the fact that the feed concentration had more effect on the power consumption than the initial transmembrane pressure or the feed flow rate, a dynamic which emphasizes as well as re-confirms the results obtained in the previous work based on the use of polycarbonate membranes with uniform pore size [14]. The average transmembrane pressure had a significant effect on the specific power consumption, a relationship that reflects the importance of accurately predicting the increase in transmembrane pressure for various membrane properties, characterizations, surface charges, and operating conditions.

3. Validation of the Attachment Models with Different Heterogeneous Membranes

We intended to examine the predictive capability of the specific power consumption model using the comprehensive set of models, which includes the mechanistic models tracking the increase in transmembrane pressure (Eq. (3)) and the models based on fouling attachments. The models were tested for a wide range of operating conditions with multiple heterogeneous membranes of different materials, MWCO values, and surface charges. At the same operating condition and the same surface charge, the power consumption would vary depending on the characteristic properties of each membrane, such as the membrane surface porosity, the pore size distribution, the number density of membrane pores per unit membrane surface area, the thickness of the membrane, and the tortuosity of the membrane pores structure, since all these parameters are considered as part of the model when it comes to the increase in transmembrane pressure. For additional depth of assessment, the models were further considered with respect to the particle size distribution of the simulated latex effluent.

Table 5 reflects partial agreement between the specific power consumption, calculated based on the experimental values, and the value predicted by the empirical model for the specific power consumption using the estimated fouling attachments and the increase in the transmembrane pressure value. The first step in

Table 5. Power consumption calculated from experimental data and the predicted values for polysulfone membranes at different operating conditions and varying membrane surface charges

Exp. No.	Operating conditions			ζ [mV]	Exp. P′	The specific power consumption [kW·h/m^3]	Predective models		Pred. * P′ (Eq. (3))	Error % P′	Predicted specific power consumption [kW·h/m^3]	Error %
	TMP [psia]	Q [LPM]	C_f [kg/m^3]				Eq. (7)	Eq. (8)				
							α_{pm}	α_{pp}				
1	15.00	1.00	0.78	−42.40	1.00	1.65	0.78	0.67	1.12	12.0	1.85	12.0
2	15.00	7.00	0.78	−42.40	0.50	1.92	0.31	0.26	0.465	−7.0	2.22	15.7
3	25.00	4.00	1.82	−42.40	7.00	8.00	0.89	0.81	7.50	7.1	6.49	−18.9
4	35.00	7.00	1.82	−42.40	6.00	7.67	0.80	0.89	6.40	6.7	8.18	6.7
5	25.00	7.00	1.30	−25.00	4.00	8.89	0.94	0.51	3.70	−7.5	7.74	−12.9
7	30.00	5.00	1.82	−15.00	6.00	9.51	0.98	0.85	6.45	7.5	7.71	−18.9
8	25.00	4.50	1.30	−28.00	6.00	6.19	0.89	0.72	5.46	9.0	5.58	−9.9

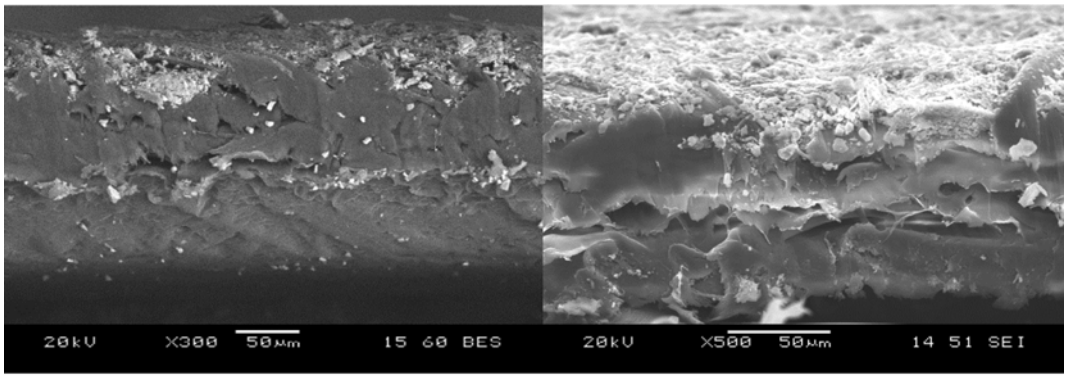

Fig. 7. SEM images of the polysulfone membrane after ultrafiltration at [P=25.00 psia], [Q=7.00 LPM], [C_f=1.30 kg/m^3] (a) with a membrane surface charge of −42.40 mV; and (b) with a membrane surface charge of −25.00 mV.

this assessment process was to accurately predict the depositional and coagulational attachments from Eqs. (7) and (8), using the initial transmembrane pressure, feed flow rate, feed concentration, and membrane surface charge values. The critical second step was to estimate the transmembrane pressure from Eq. (3), using the predicted fouling attachment, the morphological characterization of the membrane (such as the membrane surface porosity, the pore size distribution, the number density of membrane pores per unit membrane surface area, the thickness of the membrane, and the tortuosity of the membrane pores), the cumulative permeate volume per unit area, feed concentration, the particle's projected area, and the cake resistance values. The increase in transmembrane pressure was then in turn used to calculate the average transmembrane pressure throughout the filtration process, which was finally used to estimate the specific power consumption with the aid of Eq. (11). As shown in Table 5, the validation experimental runs were performed over a range of operating conditions rather than the ones used in the original experimental design and at a different polysulfone membrane surface charge values. The specific power consumption calculated from Eq. (9) and based on the experimental values agrees fairly well with the value predicted from the numerical model, with an error range of 6.7-18.9% for polysulfone membrane over varying membrane surface charges from −15.00 mV to −42.40 mV. It should be admitted that the complexity of the mechanistic model could be responsible for this error range. The mechanistic model used during the prediction of the transmembrane pressure considers the attachments of each particle size with respect to each pore size range, while in the case of the real fouling phenomenon an alternative dynamic may be executed somewhat differently. One must thus remain mindful that the model only approximates the pore size distribution ranges and does not reflect the exact pore size distribution. Consequently, the predicted increase in transmembrane pressure agreed with the experimental values with 6.7 to 12.0% error range. In addition, the experimental error occurring during the process of obtaining the experimental data would augment this deviation further, since the experimental error embedded in the data was used in the model development.

At a transmembrane pressure of 25.00 psia, a feed flow rate of 7.00 LPM, and a feed concentration of 1.30 kg/m^3, Table 3 run 12, and Table 5 run 5, respectively,show the results obtained using polysulfone membranes with surface charge of −42.40 mV and −25.00 mV. The specific increase in transmembrane pressure was 2.00 psia and 4.00 psia, in the case of polysulfone membrane with surface charges of −42.40 mV and −25.00 mV, respectively. This was due to the heightened attraction force between the latex particles and the membrane's surface, which caused a greater depositional attachment of 0.94 for polysulfone membrane with surface charge of −25.00 mV, as compared to 0.82 for polysulfone membranes with surface charge of −42.40 mV. This larger depositional attachment led to a higher total mass of fouling of 0.012 kg/m^2, as compared to 0.0088 kg/m^2. The evidence of this effect of the surface charge on the amount of fouling can be seen in the SEM images shown in Fig. 7. A lower cumulative permeate volume per unit area of 0.042 m^3/m^2 was obtained with the polysulfone membrane with a lower surface charge of −25.00 mV. For the polysulfone membrane with a hydrophilic surface (zeta potential of −42.40 mV) the cumulative permeate volume per unit area was 0.113 m^3/m^2. As a consequence, the specific power consumption values were 3.33 kW·h/m^3 and 8.89 kW·h/m^3 for polysulfone membranes with surface charges of −42.40 mV and −25.00 mV, respectively. This result effectively confirmed our expectations since the cumulative permeate volume is inversely proportional to the specific power consumption, as indicated in Eq. (9). Also, the model incorporates surface charge influence on the depositional attachment in addition to the cumulative permeate volume per unit area, making this model a reliable prediction tool for accurately evaluating the power consumption.

In addition, Ultrafilic and PVDF membranes with an MWCO of 100,000, and cellulose acetate membranes with an MWCO of 20,000, were specifically tested. Table 6 shows the predicted power consumption using various membranes at different operating conditions, which agreed with the power consumption calculated from the experimental values and featured an error margin range of 6.0% to 19.1%. Notably, the predicted increase in transmembrane pressure agreed with the experimental value within the error range of 4.7 to 12.3%.

As shown in Table 6, for experimental run number 4 with cellulose acetate at a transmembrane pressure of 25.00 psia, feed flow

Table 6. Power consumption calculated from on the experimental data and predicted values for various membranes at different operating conditions

Exp. no.	Membrane	Operating conditions			ζ [mV]	Exp. P′	The specivic power consumption [kW·h/m^3]	Predective models		Pred. * P′ (Eq. (3))	Error % P′	Predicted specific power consumption [kW·h/m^3]	Error %
		TMP [psia]	Q [LPM]	C_f [kg/m^3]				Eq. (7) α_{pm}	Eq. (8) α_{pp}				
1	UF	35.00	7.00	1.82	−41.50	8.50	7.19	0.82	0.84	8.10	−4.7	8.46	17.7
2	UF	25.00	4.50	2.34	−41.50	10.00	8.92	0.98	0.99	10.78	7.8	7.22	−19.1
3	UF	15.00	7.00	1.30	−41.50	2.00	3.22	0.19	0.29	2.20	10.0	3.42	6.0
4	CA	25.00	4.00	1.30	−33.90	1.50	5.84	0.81	0.76	1.33	−11.3	4.92	−15.8
5	CA	35.00	7.00	1.82	−33.90	2.00	9.11	0.88	0.84	2.12	6.0	7.99	−12.2
6	PVDF	15.00	7.00	0.78	−2.50	4.50	4.36	0.92	0.24	4.10	−8.9	3.63	−16.8
7	PVDF	15.00	7.00	1.30	−2.50	5.50	6.08	0.98	0.30	4.98	−9.5	5.01	−17.5
8	PVDF	20.00	4.00	0.26	−2.50	4.00	4.39	0.99	0.57	3.51	−12.3	3.85	−12.4

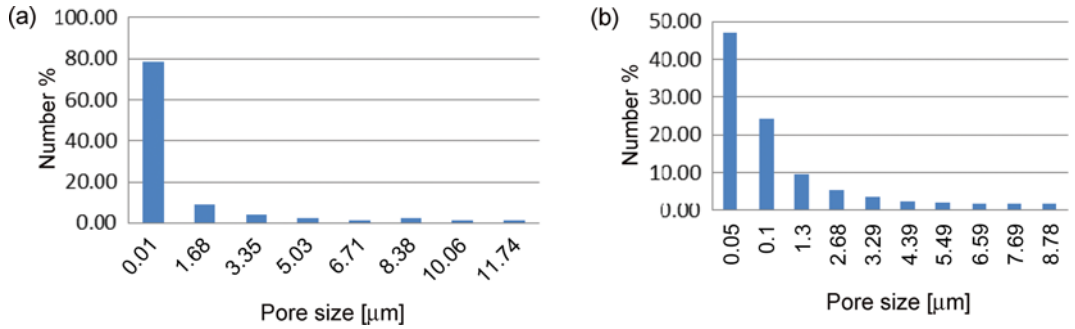

Fig. 8. The pore size distribution (a) cellulose acetate (b) polysulfone membrane.

rate of 4.00 LPM and feed concentration 1.30 kg/m^3, the increase in transmembrane pressure was 1.50 psia, while the power consumption was 5.84 kW·h/m^3. At the same operating conditions with polysulfone membrane (Table 3, run 15), the increase in transmembrane pressure was 5.00 psia and the specific power consumption was 2.04 kW·h/m^3. The surface charges of polysulfone and cellulose acetate membranes are relatively close to each other at −42.40 mV and −33.90 mV, respectively. Alternatively, cellulose acetate membranes with an MWCO of 20,000 featured 80% of the pore size distribution at 0.01 microns, as presented in Fig. 8(a), which caused the lower experimental mass of fouling and smaller increase in transmembrane pressure. Increasing the pore size in case of polysulfone membranes with MWCO of 60,000, as shown in Fig. 8(b), facilitated a higher flow through the membrane's pores, effectively raising the chances for particle-to-particle and particle-to-membrane collisions and attachments, and promoting pore blocking. As a result, both the mass of fouling and the transmembrane pressure increased over the filtration period. However, the permeate volume was higher with polysulfone membrane, which resulted in a lower specific power consumption. Fig. 9 shows the SEM images after the ultrafiltration process using cellulose acetate and polysulfone membranes, at a transmembrane pressure of 25.00 psia, feed flow rate of 4.00 LPM, and feed concentration of 1.30 kg/m^3. What stands out in this case study is the fact that latex particles appeared to penetrate deeper inside the pores of polysulfone membrane, as compared to the case of cellulose acetate membranes. By engaging with these results, the overall experimental direction again emphasizes the effects of the morphological characterization of the membrane on the specific power consumption.

Another case study to analyze can be viewed in run 3 in Table 3 and run 6 in Table 6, both of which show the results obtained using polysulfone membranes and PVDF membranes at the transmembrane pressure of 15.00 psia, the feed flow rate of 7.00 LPM, and the feed concentration of 0.78 kg/m^3. The increase in transmembrane pressure was 0.50 psia and 4.50 psia for polysulfone and PVDF membranes, respectively. Similarly, the specific power consumption was 1.92 kW·h/m^3 and 4.36 kW·h/m^3 for polysulfone and PVDF membranes. A PVDF membrane with MWCO of 100,000 has the majority of larger pore sizes, as compared to those of a polysulfone membrane with MWCO of 60,000. The pore size distribution had a significant effect on the mass of fouling retained by the membrane and caused the increase in transmembrane pressure, resulting in the differences in the specific power consumption values and the transmembrane pressure augmentation of the two membranes. Moreover, the higher negative charge of polysulfone membranes of −42.40 mV generated a greater level of repulsion force between particles and the membrane's surface, if compared to PVDF membrane with surface charge of −2.50 mV. Note that the depositional attachment was 0.35 and 0.92 for polysulfone and PVDF membrane, respectively. Consequently, the total mass of fouling and the average transmembrane pressure values were higher for PVDF at the same operating conditions.

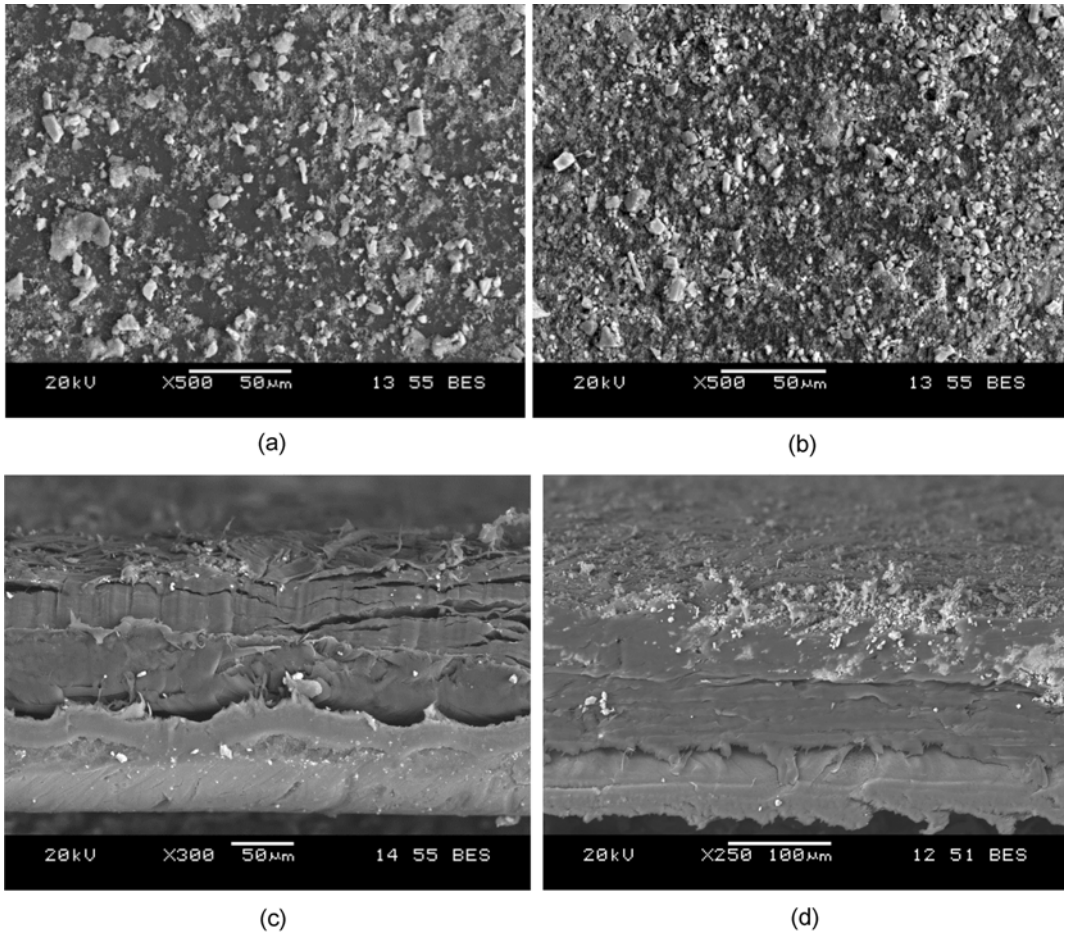

Fig. 9. SEM images after ultrafiltration at [P=25.00 psia], [Q=4.00 LPM], [C_f=1.30 kg/m^3] using (a) membrane surface of cellulose acetate membrane with MWCO of 20,000; (b) membrane surface of polysulfone membrane with MWCO of 60,000; (c) side view of the cake height using cellulose acetate membrane with MWCO of 20,000; (d) side view of the cake height of polysulfone membrane with MWCO of 60,000.

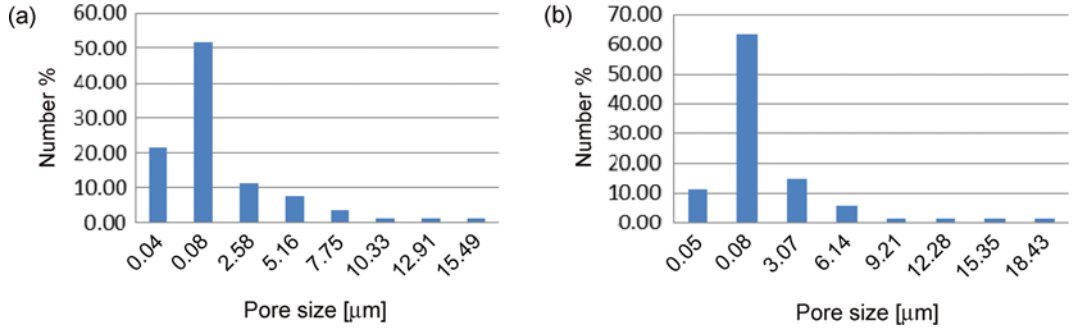

Fig. 10. The pore size distribution (a) ultrafilic membrane and (b) PVDF membrane.

Even though both Ultrafilica and PVDF membranes have the same MWCO of 100,000 and feature similar pore size distribution (Fig. 10), the surface charges of each membrane played a critical role in the fouling attachments and the total mass of fouling, resulting in a higher increase in transmembrane pressure and lower cumulative permeate volume. For example, at the transmembrane pressure of 15.00 pisa, the feed flow rate of 7.00 LPM, and feed concentration of 1.30 kg/m^3 (Table 6 runs 3 and 7), the increase in transmembrane pressure was 2.00 psia and 5.50 psia for Ultrafilic and PVDF membranes, respectively. This particular dynamic can be attributed to the higher negative surface charge of −41.50 mV for Ultrafilic membranes compared to 2.50 mV for hydrophobic PVDF membranes. The depositional attachment values were thus 0.19 and 0.98 for Ultrafilic and PVDF membranes, respectively. As a consequence, the total mass of fouling was 0.014 kg/m^2 for PVDF and 0.0092 kg/m^2 for Ultrafilic membranes. Critical visual obser-

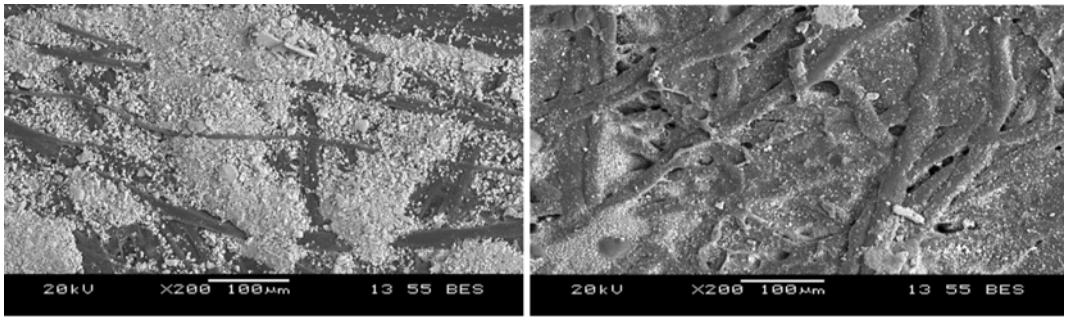

Fig. 11. SEM images after ultrafiltration at [P=15.00 psia], [Q=7.00 LPM], [C_f=1.30 kg/m^3] using (a) PVDF membrane with zeta potential of −2.50 mV; (b) ultrafilic membrane with zeta potential of −41.50 mV.

vations of the deposit on the membranes can be found in Fig. 11. Furthermore, the cumulative permeate volume was 0.07 m^3/m^2 and 0.04 m^3/m^2 for Ultrafilic and PVDF membranes, respectively. The specific power consumption for Ultrafilic membrane (3.22 kW·h/m^3) was lower than that of PVDF (6.08 kW·h/m^3) as expected. In addition, the predicted respective transmembrane pressure using Ultrafilic and PVDF was 2.20 and 4.10 psia. This key differentiation stems from a variety of reasons, including the surface hydrophilic, which had a significant impact on the depositional attachment and the cumulative permeate flux, both of which in turn affected the predicted augmentation of the transmembrane pressure. This difference can likewise be connected to the fact that even though both membranes have MWCO of 100,000, they feature different pore size distribution (Fig. 10), and the model considers the attachment analyses of each particle size in correspondence to each pore size. Accordingly, these resulting predictions of the transmembrane pressure enhanced the model's overall accuracy with the variation of the morphological characterization of each membrane. Thus, the prediction of the increase in transmembrane pressure using this comprehensive model is accurate and highly practical when it comes to real case scenarios. This model indicates a remarkably good prediction correlation for heterogeneous membranes featuring various materials, MWCO values, and surface charges.

Consider Table 7, which shows the experimental runs performed in order to comprehensively test and validate the ability of the complete set of the predictive models to accurately estimate the power consumption at a required cumulative permeate volume. In the previous sections, the models were validated using the cumulative permeate volume obtained experimentally. On the other hand, Table 7 presents the predicted power consumption based on an arbitrarily required cumulative permeate volume V_s for the untreated polysulfone membrane with surface charge of −42.40 mV. The predicted values obtained through the model agree with the power consumption calculated from the experimental data of the cumulative filtrate volume within an error range of 7.5 to 17.1%. Similarly, the predicted increase in transmembrane pressure corresponds to the experimental value with an error value ranging from 4.3 to 11.7%. Based on this assessment, the models can be considered as reasonably accurate when it comes to predicting the membrane's performance.

For practical use in an industrial setting, the specific power consumption can be predicted for a membrane filtration process, using the operating conditions, membrane surface charge, and the morphological characterization of the heterogeneous membrane. The depositional attachment and the coagulation attachment can be estimated from Eq. (7) and Eq. (8). The fouling attachments in addition to the morphological characterization of the membrane can be, in turn, employed to accurately estimate the increase in the transmembrane pressure at a required cumulative permeate volume per unit area.

CONCLUSION

This extensive case-based study examined the predictive capa-

Table 7. Predicted power consumption using the arbitrarily input cumulative permeate volume V_s and the power consumption calculated from the experimental cumulative permeate volume for polysulfone membranes

Exp. No.	Operating conditions			V_s [L]	Exp. P′	The specific power consumption [kW·h/m^3]	Predective models		Pred. * P′ (Eq. (3))	Error % P′	Predicted specific power consumption [kW·h/m^3]	Error %
	TMP [psia]	Q [LPM]	C_f [kg/m^3]				Eq. (7) α_{pm}	Eq. (8) α_{pp}				
1	30.00	2.00	1.30	0.50	5.00	5.89	0.89	0.88	4.65	−7.0	5.30	−10.0
2	25.00	7.00	1.82	2.00	5.00	4.58	0.84	0.72	5.55	11.0	5.17	13.0
3	35.00	2.00	1.82	0.50	3.00	6.41	0.93	0.87	2.65	−11.7	5.93	−7.5
4	15.00	4.00	1.30	1.50	3.00	1.99	0.66	0.55	2.87	−4.3	2.29	15.2
5	20.00	4.00	0.78	1.50	3.00	2.78	0.80	0.33	3.28	9.3	3.26	17.1

bility of the specific power consumption empirical model through the use of the complete set of models, including mechanistic models based on the increase in transmembrane pressure and the correlations of fouling attachments. This highly developed model incorporated the fouling attachment as well as the chemical and physical factors in membrane fouling to guarantee an accurate prediction and scale-up application. The model could be applied to both hydrophilic and hydrophobic heterogeneous membranes with non-uniform pore size at a given operating condition, and with a specified membrane surface charge value. The developed numerical models contribute to merging an existing research gap by predicting the power consumption in ultrafiltration of simulated latex effluent for a variety of operating conditions with diversified heterogeneous membranes featuring different materials, MWCO values, and surface charges.

The numerical model of specific power consumption agreed well with the power consumption calculated based on the experimental values for both hydrophilic and hydrophobic membranes of various materials and different MWCO with an error range of 6.0 to 19.1%. Alternatively, the increase in transmembrane pressure corresponded with the experimental values with error margin of 4.7 up to 12.3%. We successfully tested the complete set of models necessary for the prediction of the specific power consumption with respect to the required membrane performance signifiers necessary for the model's calculations. The results of these experimental case studies indicate that the morphological characterization of the membrane, operating conditions, and membrane surface charge have a potent effect on the specific power consumption, and play a critical role that both justifies and encourages their inclusion into the complete set of predictive models at the core of current membrane research.

ACKNOWLEDGEMENTS

The authors are grateful for the financial support from the Natural Science and Engineering Research Council of Canada (NSERC). The assistance and facilities provided by the Department of Chemical Engineering, Ryerson University, have made this research possible and are also highly appreciated.

NOMENCLATURE

Symbol Description

- a : particle radius [m]
- B_i : mass transfer coefficient through the pore size [m^{-2}]
- β : model coefficient
- β_{ko} : the intercept of the linear model
- β_{ki} : te first-order model coefficients
- C_f : concentration of foulants in the feedwater [kg/m^3]
- D : the diffusion coefficient of colloidal particles [m^2/s]
- D_{m_i} : membrane pore diameter of size [m]
- L_m : length of membrane pores [m]
- m_p : mass of particles attaching to membrane pores in a unit membrane surface area [kg/m^2]
- m_{pL_i} : mass of the particles larger than the pore of size contribute to pore blocking [kg/m^2]
- m_{pS_i} : mass of small particles attaching to membrane pores of size in a unit membrane surface area [kg/m^2] ($D_{m_i}/6$<particle size<$D_{m_i}/2$)
- m_c : the total mass of particles in the cake layer per unit membrane surface area [kg/m^2]
- m_t : the total mass of particles retained per unit membrane surface area [kg/m^2]
- m_{w_i} : mass of the particles attaching to the pore walls of size i normalized to unit membrane surface area [kg/m^2] (particle size<$D_{m_i}/6$)
- N : the total number of the non-uniform pore sizes determined in the pore size distribution of the heterogeneous membranes
- N_m : the number density of membrane pores per a unit membrane surface area
- P-value : probability in statistical significance testing (ANOVA test)
- R^2 : the percent of the variation of the response explained by the model
- $\hat{R}_c$: the resistance due to the cake layer [m/kg]
- R_m : the membrane's resistance [m^{-1}]
- TMP : initial transmembrane pressure [psia]
- $\overline{TMP}_{AVG}$: time-averaged transmembrane pressure throughout the filtration duration [psia·min]
- Q : feed flow rate [L/min]
- V_s : the cumulative volume of the permeate normalized to membrane surface area [m^3/m^2]
- $\overline{V}_s$: cumulative permeate volume [m^3]
- x_i : number average percentage of the pore of size i
- X_i : the i^{th} independent factor
- Y : the response factor of the specific power consumption
- σ : projected area of a unit mass of the particles on membrane surface [m^2/kg]
- σ_L : projected area of a unit mass of the large particles (particle diameter≥pore diameter) on membrane surface [m^2/kg]
- σ_S : the projected area of a unit mass of the small particles on the membrane surface [m^2/kg] (pore diameter/6<particle radius<pore diameter/2)
- σ_{XS} : projected area of a unit mass of the very small particles on membrane surface [m^2/kg] (particle radius<pore diameter/6)
- ε_s : membrane surface porosity [dimensionless]
- α_{pm} : the attachment probabilities between a particle and the membrane [dimensionless]
- α_{pp} : the attachment probabilities between two particles [dimensionless]
- τ : tortuosity of the membrane [dimensionless]

REFERENCES

1. M. Kennedy, J. Kamanyi, S. Rodriguez, N. Lee, J. Schippers and G. Amy, *Adv. Membr. Technol. Appl.*, 131 (2008).
2. M. H. Javacek and F. Bouchet, *J. Membr. Sci.*, **82**, 285 (1993).
3. R. Thiruvenkatachari, W. G. Shim, J. W. Lee and H. moon, *Korean J. Chem. Eng.*, **22**(2), 250 (2205).
4. S. Kosvintsev, I. W. Cumming, R. G. Holdich, D. Lloyd and V. M. Starov, *Colloids Surf., A*, **230**, 167 (2004).
5. J. lozier and A Jacangelo, Where we are head ? - the future of membrane treatement, *in Proceedings of Water Quality Tech-*

nology Conference, November 10-14, 2002, Seattle, WA.
6. A. Al-Amoudi and R.W. Lovitt, *J. Membr. Sci.*, **303**, 4 (2007).
7. A. Hu and D. Stuckey, *J. Environ. Eng.*, **132**(2), 190 (2006).
8. H. B. Winzeler and G. Belfort, *J. Membr. Sci.*, **80**, 35 (1993).
9. S. A. Avlonitis, K. Kouroumbas and N. Vlachakis, *Desalination*, **157**, 151 (2003).
10. A. H. Bahnasawy and M. E. Shenana, *Aust. J. Agric. Eng.*, **15**, 54 (2010).
11. D. Suman, S. Projjwal, B. Chiranjib and D. Siddhartha, *J. Environ. Pollut.,* **49**(3-4), 197 (2012).
12. J. Jurado and B. J. Bellhouse, *Filtr. Sep.*, 273 (1994).
13. F. Knops and H Futselaar, *J. Membr. Sci.*, **73**, 153 (1992).
14. A. Abdelrasoul, H. Doan and A. Lohi, *Can. J. Chem. Eng.*, **92**(7), 1293 (2014).
15. A. Abdelrasoul, H. Doan, A. Lohi and C.-H. Cheng, *Ind. Eng. Chem. Res.*, **53**, 9897 (2014).
16. A. Abdelrasoul, H. Doan, A. Lohi and C.-H. Cheng, *Sep. Purif. Technol.*, **135**, 199 (2014).
17. A. Abdelrasoul, H. Doan and A. Lohi, *J. Membr. Sep. Technol.*, **2**, 134 (2013).
18. A. Abdelrasoul, H. Doan and A. Lohi, Fouling in Membrane Filtration and Remediation Methods, *Mass Transfer - Advances in Sustainable Energy and Environment Oriented Numerical Modeling*, Dr. Hironori Nakajima (Ed.), Intech Open Access Publisher, 195 (2013).
19. A. Abdelrasoul, H. Doan and A. Lohi, *J. Membr. Sci.*, **433**, 88 (2013).
20. A. Abdelrasoul, H. Doan, A. Lohi and C.-H. Cheng, *Can. J. Chem. Eng.* (2014), DOI:10.1002/cjce.22056.
21. D. C. Montgomery, *Design and Analysis of Experiment*, 5th Ed., Wiley, Inc., New York, USA (1997).